Short Papers

The Chaotic Mobile Robot

Yoshihiko Nakamura and Akinori Sekiguchi

***Abstract*—In this paper, we develop a method to impart the chaotic nature to a mobile robot. The chaotic mobile robot implies a mobile robot with a controller that ensures chaotic motions. Chaotic motion is characterized by the topological transitivity and the sensitive dependence on initial conditions. Due to the topological transitivity, the chaotic mobile robot is guaranteed to scan the whole connected workspace. For scanning motion, the chaotic robot neither requires the map of the workspace nor plans the global motion. It only requires the measurement of the local normal of the workspace boundary when it comes close to it. We design the controller such that the total dynamics of the mobile robot is represented by the Arnold equation, which is known to show the chaotic behavior of noncompressive perfect fluid. Experimental results and their analysis illustrate the usefulness of the proposed controller.**

***Index Terms*—Arnold equation, chaos, mobile robot.**

I. Introduction

Chaos characterizes one of mysterious rich behaviors of nonlinear dynamical systems. Many research efforts have been paid to establish the mathematical theory behind chaos. Applications of chaos are also being studied and include, for example, controlling chaos [1]–[4] and chaotic neural networks [5]–[8].

This paper proposes a method to impart chaotic behavior to a mobile robot. This is achieved by designing a controller which ensures chaotic motion. The topological transitivity[1] property of chaotic motions guarantees a complete scan of the whole connected workspace. The proposed scheme neither requires a map of the workspace nor plans a path through it. It only requires the measurement of the local normal of the boundary when it comes close to it.

A mobile robot with such characteristics may find its applications as a patrol robot or a cleaning robot in a closed room, floor, or building (Fig. 1). The sensitive dependence on initial condition also yields a favorable nature as a patrol robot since the scanning trajectory becomes highly unpredictable.

II. Chaotic Mobile Robot With the Arnold Equation

A. Mobile Robot

As the mathematical model of mobile robots, we assume a two-wheeled mobile robot as shown in Fig. 2. Let the linear velocity of the robot v [m/s] and the angular velocity ω [rad/s] be the inputs to the system. The state equation of the mobile robot is written as follows:

$$\begin{pmatrix} \dot{x} \\ \dot{y} \\ \dot{\theta} \end{pmatrix} = \begin{pmatrix} \cos\theta & 0 \\ \sin\theta & 0 \\ 0 & 1 \end{pmatrix} \begin{pmatrix} v \\ \omega \end{pmatrix} \tag{1}$$

where (x [m], y [m]) is the position of the robot and θ [rad] is the angle of the robot.

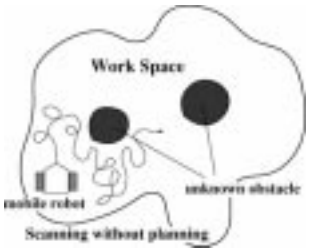

Fig. 1. Chaotic patrol.

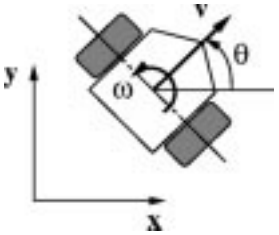

Fig. 2. Mobile robot.

B. The Arnold Equation

In order to generate chaotic motions of the mobile robot, we employ the Arnold equation, which is written as follows:

$$\begin{pmatrix} \dot{x}_1 \\ \dot{x}_2 \\ \dot{x}_3 \end{pmatrix} = \begin{pmatrix} A\sin x_3 + C\cos x_2 \\ B\sin x_1 + A\cos x_3 \\ C\sin x_2 + B\cos x_1 \end{pmatrix} \tag{2}$$

where A, B, and C are constants. The Arnold equation describes a steady solution to the three-dimensional (3-D) Euler equation

$$\frac{\partial v_i}{\partial t} + \sum_{k=1}^{3} v_k \frac{\partial v_i}{\partial x_k} = -\frac{1}{\rho}\frac{\partial p}{\partial x_i} + f_i \tag{3}$$

$$\sum_{i=1}^{3} \frac{\partial v_i}{\partial x_i} = 0 \tag{4}$$

which expresses the behaviors of noncompressive perfect fluids on a 3-D torus space. (x_1, x_2, x_3) and (v_1, v_2, v_3) denote the position and velocity of a particle and p, and (f_1, f_2, f_3) and ρ denote the pressure, external force, and density, respectively. It is known that the Arnold equation shows periodic motion when one of the constants, for example C, is 0 or small and shows chaotic motion when C is large [9].

1) The Poincaré Section: We compose Poincaré sections [10] of the Arnold equation by numerical computation. The results are shown in Figs. 3–5. The sections and coefficients of the Arnold equation are shown in Table I. Figs. 6 and 7 show trajectories of the Arnold equation in a 3-D torus space, corresponding to Figs. 3 and 5, respectively.

Manuscript received August 14, 2000; revised August 15, 2001. This paper was recommended for publication by Associate Editor L. Kavraki and Editor A. De Luca upon evaluation of the reviewers' comments. This work was supported by the CREST Program of the Japan Science and Technology Corporation under "Robot Brain Project" (PI: Y. Nakamura, Univ. of Tokyo).

Y. Nakamura is with the Department of Mechano-Informatics, University of Tokyo, Tokyo 113-0033, Japan, and also with the CREST, Japan Science and Technology.

A. Sekiguchi is with the Department of Mechano-Informatics, University of Tokyo, Tokyo 113-0033, Japan.

Publisher Item Identifier S 1042-296X(01)11161-4.

[1]Consider $\boldsymbol{C}^r(r \geq 1)$ autonomous vector fields on $\boldsymbol{R}^n$ denoted as $\dot{x} = f(x)$. Let the flow generated by this equation be denoted as $\phi(t, x)$ and let $\Lambda \subset \boldsymbol{R}^n$ be a invariant compact set for this flow. A closed invariant set Λ is said to be topologically transitive [10] if, for any two open sets $U, V \subset \Lambda$, $^{\exists}t \in \boldsymbol{R}$, $^{\exists}\phi(t, U) \cap V \neq \emptyset$.

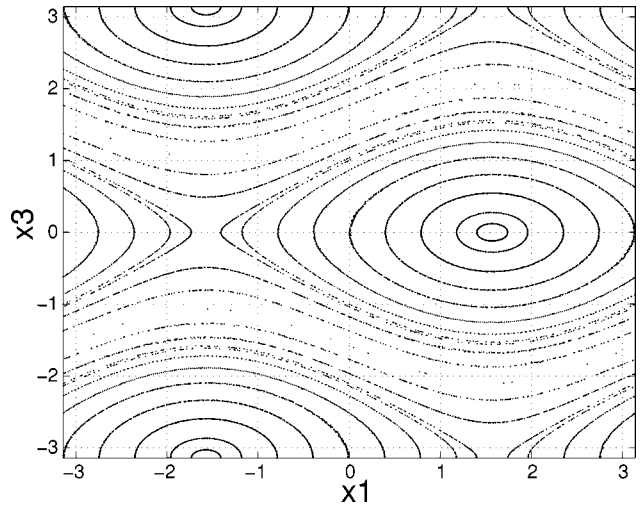

Fig. 3. Poincaré section of Arnold flow ($A = 1,\ B = 0.5,\ C = 0$).

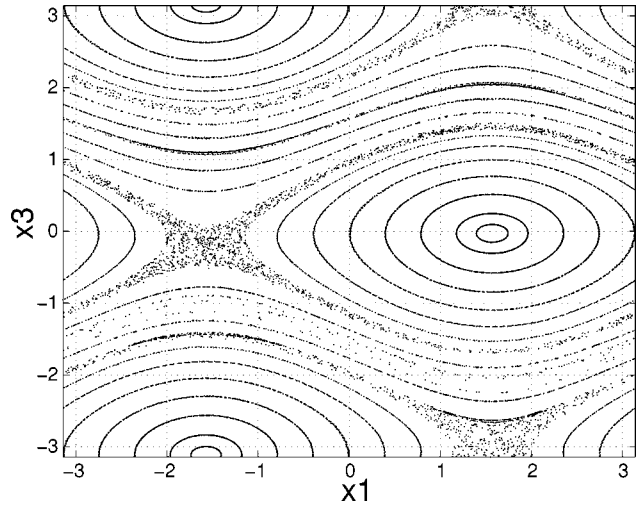

Fig. 4. Poincaré section of Arnold flow ($A = 1,\ B = 0.5,\ C = 0.05$).

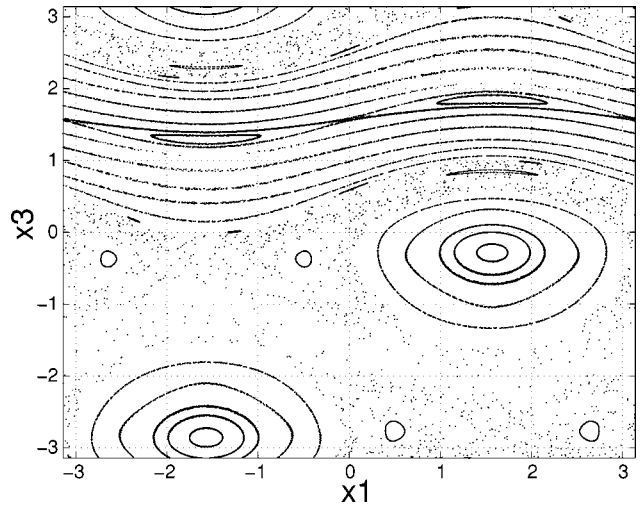

Fig. 5. Poincaré section of Arnold flow ($A = 1,\ B = 0.5,\ C = 0.5$).

Fig. 3 represents the Poincaré section when $C = 0$. It is observed that the topological transitivity does not emerge in this case, since trajectories in the Poincaré section are closed. When $|C|$ exceeds a certain small number and gets larger, there grow regions in which closed trajectories disappear and scattered discrete points appear. The regions characterize chaos and its behavior. Since the Arnold equation is a conservative system, it is an important feature that the descrete trajectory of a point initially started in such a region remains there and is never attracted by the closed trajectories outside the region.

TABLE I
PARAMETERS FOR COMPUTATIONS

	coefficients	section
Fig.3	$A = 1, B = 0.5, C = 0$	$x_2 = 0$
Fig.4	$A = 1, B = 0.5, C = 0.05$	
Fig.5	$A = 1, B = 0.5, C = 0.5$	

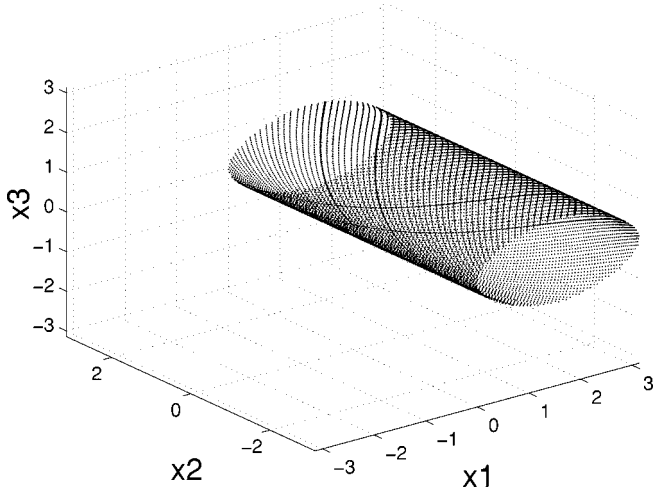

Fig. 6. Arnold flow ($A = 1,\ B = 0.5,\ C = 0$).

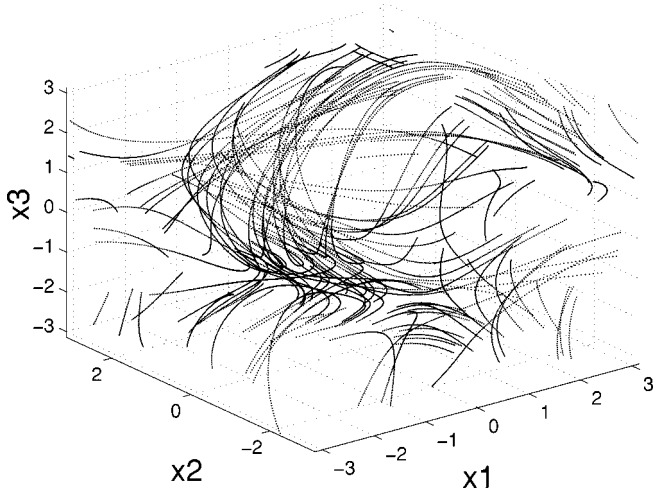

Fig. 7. Arnold flow ($A = 1,\ B = 0.5,\ C = 0.5$).

2) The Lyapunov Exponent: The Lyapunov exponent is used as a measure of the sensitive dependence on initial conditions, that is, one of two characteristics of chaotic behavior [11]. There are n Lyapunov exponents in an n-dimensional state space and the system is concluded to have the sensitive dependence on initial conditions when the maximum Lyapunov exponent is positive.

We calculated the Lyapunov exponents of the Arnold equation, using the method proposed by Shimada and Nagashima [12]. The parameters and the initial states are as follows:

$$coefficients : A = 0.5, B = 0.25, C = 0.25$$
$$initial\ states : x_1 = 4, x_2 = 3.5, x_3 = 0$$

and the Lyapunov exponents are

$$\lambda_1 = 4.3 \times 10^{-2}$$
$$\lambda_2 = 1.1 \times 10^{-4}$$
$$\lambda_3 = -4.3 \times 10^{-2}.$$

Since the maximum exponent λ_1 is positive, the Arnold equation has the sensitive dependence on initial conditions.

In case of the Arnold flow, the sum of the Lyapunov exponents, $\lambda_1 + \lambda_2 + \lambda_3$, equals zero since the volume in the state space is conserved. This results in the fact that a trajectory which started from a chaotic region will not be attracted into attractors like limit cycles. The total of the computed Lyapunov exponents became slightly larger than zero, which is due to the numerical computation error.

C. Integration of the Arnold Equation

In order to integrate the Arnold equation into the controller of the mobile robot, we define and use the following state variables:

$$\begin{cases} \dot{x_1} = D\dot{y} + C\cos x_2 \\ \dot{x_2} = D\dot{x} + B\sin x_1 \\ x_3 = \theta \end{cases} \tag{5}$$

where B, C, and D are constants. Substituting (1) into (5), we obtain a state equation on x_1, x_2 and x_3 as follows:

$$\begin{cases} \dot{x_1} = Dv + C\cos x_2 \\ \dot{x_2} = Dv + B\sin x_1 \\ \dot{x_3} = \omega \end{cases}. \tag{6}$$

We now design the inputs as follows:

$$\begin{cases} v = \frac{A}{D} \\ \omega = C\sin x_2 + B\cos x_1 \end{cases}. \tag{7}$$

Consequently, the state equation of the mobile robot becomes

$$\begin{pmatrix} \dot{x}_1 \\ \dot{x}_2 \\ \dot{x}_3 \\ \dot{x} \\ \dot{y} \end{pmatrix} = \begin{pmatrix} A\sin x_3 + C\cos x_2 \\ B\sin x_1 + A\cos x_3 \\ C\sin x_2 + B\cos x_1 \\ v\cos x_3 \\ v\sin x_3 \end{pmatrix}. \tag{8}$$

Equation (8) includes the Arnold equation. The Arnold equation behaves chaotically or not, depending upon the initial states. We choose the initial states of the Arnold equation such that the trajectory should behave chaotically. As explained in Section II-B, it is guaranteed that a chaotic orbit of the Arnold equation is not attracted to a limit cycle or a quasi-periodic orbit.

The whole states evolve in a 5-D space according to (8), which includes a 3-D subspace of the Arnold flow. The state evolution in the 2-D complementary space is highly coupled with that in the 3-D subspace as seen in (8). The coupling is physically interpreted by the fact that the mobile robot moves with a constant velocity and being steered by the third variable of the Arnold equation. Although it is likely that the trajectory in the x–y space also behaves chaotic, it is difficult to prove. The nature of the mobile robot trajectory is to be numerically evaluated in the following section.

The inputs to the mobile robot become continuous since the Arnold equation is a continuous system. Though the Rössler equation, the Lorenz equation, and so on are well known as low-dimensional continuous chaotic systems, the Arnold equation has some advantages as follows.

- The structures of the Arnold equation and the mobile robot equation are similar.
- It is easy to deal with because the state variables x_1, x_2, and x_3 are limited within a 3-D torus space.
- The range of the input ω becomes $-(|B|+|C|) \le \omega \le |B|+|C|$ and suitable for a robot input.
- The maximums of $|\dot{x}_1|, |\dot{x}_2|, |\dot{x}_3|$ are determined by the parameters A, B, and C.

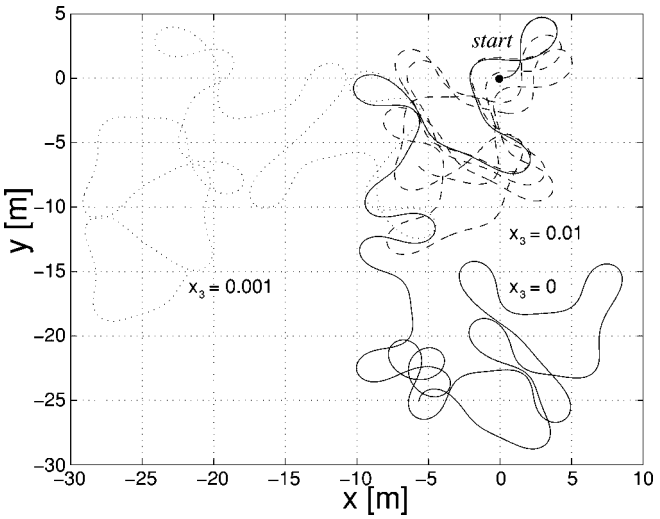

Fig. 8. Trajectories of the mobile robot in x-y plane ($v = 1,\ A = 1,\ B = 0.5,\ C = 0.5$).

D. Mirror Mapping

Fig. 8 shows an example of motions of the mobile robot with the proposed controller, obtained by numerical simulation. The initial condition was chosen from a region where the Poincaré section forms no closed trajectory. It is observed that the motion of the robot is unpredictable and sensitively dependent on initial conditions.

In (8), it is assumed that the robot moves in a smooth state space with no boundary. However, a real robot moves in spaces with boundaries like walls or surfaces of obstacles. To solve this problem, we consider the motion of the robot in an imaginary space as shown in Fig. 9. This imaginary space is obtained by smoothly connecting boundaries of two spaces that have the same shape as the real space.

In Fig. 9, the real space has a topologically circular shape. The real space is assumed to be a closed space and placed on another imaginary space with an equivalent shape to the real one in such a way that every corresponding pair of points on the two spaces meet. The two spaces are glued and connected on the boundaries. Blowing air in between the surfaces and allowing elastic deformation, we obtain a smooth manifold as shown in the top-left figure in Fig. 9, where the robot can move between the two sides smoothly at the boundaries. The mobile robot moves on the surface of the manifold in the mathematical model of the work space, while in the real space it moves as if we observe its motion in the mathematical model through the transparent manifold from the above. However, note that, for the observation through the transparent manifold, we have to apply coordinate transformation from the left-hand system to the right-hand system. This is why we call it mirror mapping. In the real space, the mobile robot moves as if it is reflected by the boundary.

III. Numerical Analysis of the Behavior of the Robot

We investigate by numerical analysis whether the mobile robot with the proposed controller actually behaves in a chaotic manner. Examples of trajectories of the robot are obtained by applying the mirror mapping and are shown in Figs. 10 and 11. The parameters and the initial states

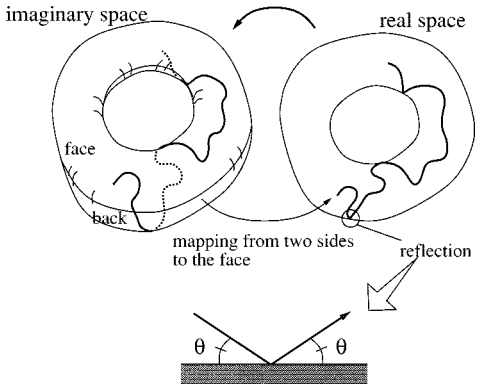

Fig. 9. Mirror mapping.

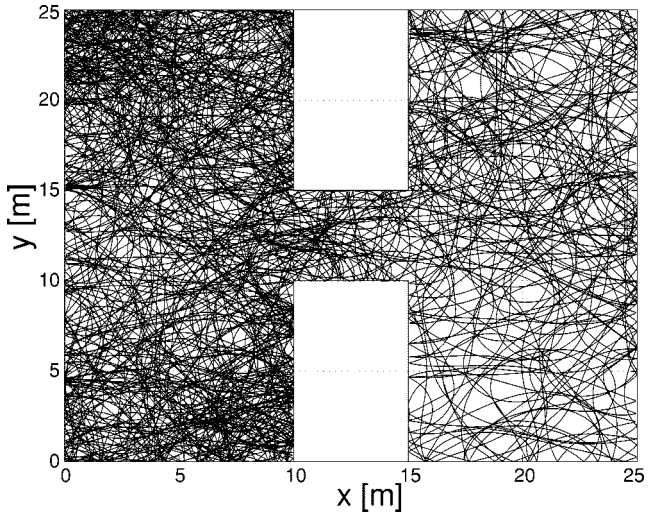

Fig. 10. Simulated trajectory of the mobile robot in the x–y plane (Environment 1).

used are as follows:

$$\begin{aligned} coefficients: v &= 1\ [\text{m/s}], A = 0.5\ [1/\text{s}], \\ B &= 0.25\ [1/\text{s}], C = 0.25\ [1/\text{s}] \\ initial\ states: x_1 &= 4, x_2 = 3.5, \\ x_3 &= 0, x = 5\ [\text{m}], y = 5\ [\text{m}] \\ period: &\quad 8000\ [\text{s}]. \end{aligned}$$

The trajectories generated by (8) scanned the whole workspace regardless of the shape of workspace. The trajectories from other initial positions of the robot scan the whole workspace similarly. The coefficients and the initial state of the Arnold equation are chosen so that the trajectory should behave chaotic. For example, we choose an initial state from the regions in which scattered discrete points appear in the Poincaré map of the Arnold equation. Though the magnitude of the coefficients would affect the efficiency of scanning the workspace, it is not difficult to choose appropriate magnitude of the coefficients since the Arnold equation accelerate or slow down its motion with the same shape of trajectories when the magnitude of the coefficients are changed with a fixed ratio $A : B : C$.

Figs. 12 and 13 show the Poincaré sections at $x_3 = \pi/4$ obtained from Figs. 10 and 11. The descrete points are distributed over the whole workspace, which indicates that the motion generated by the proposed controller shows the topological transitivity in the workspaces.

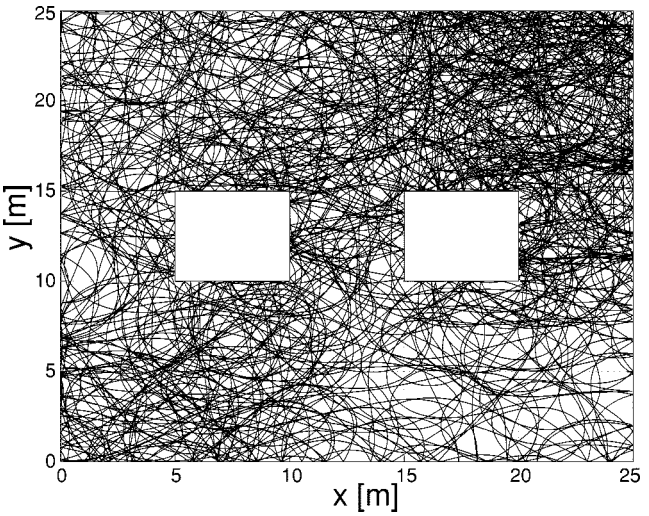

Fig. 11. Simulated trajectory of the mobile robot in the x–y plane (Environment 2).

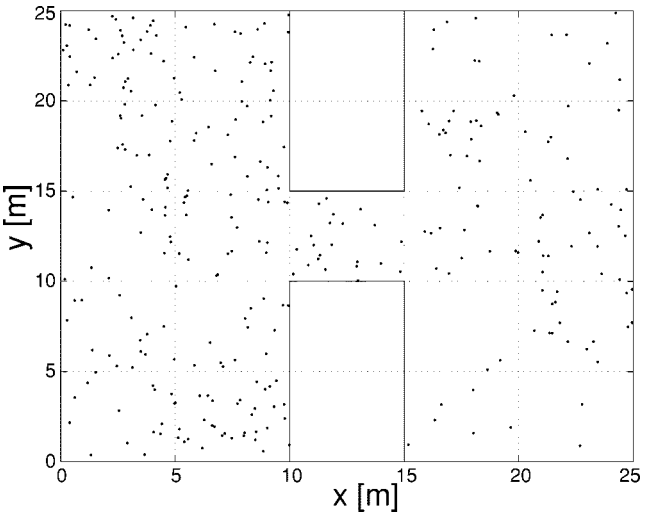

Fig. 12. Poincaré map of the simulation (Environment 1).

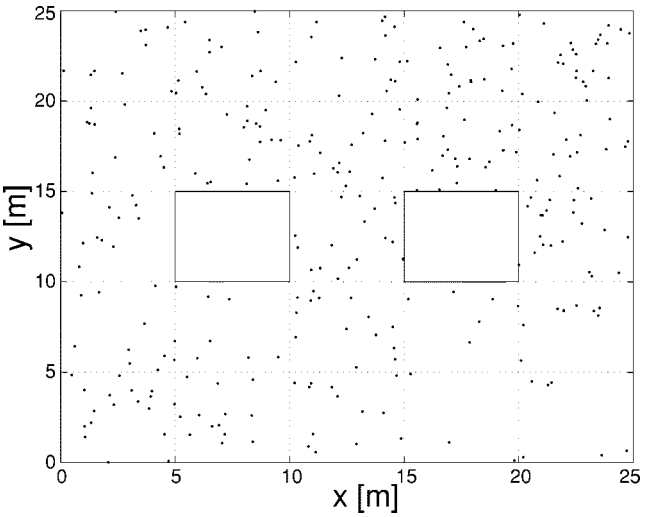

Fig. 13. Poincaré map of the simulation (Environment 2).

We calculated the Lyapunov exponents of the robot. Three Lyapunov exponents on the trajectory in 3-D space (x, y, x_3), projected from 5-D

Fig. 14. Prototype mobile robot.

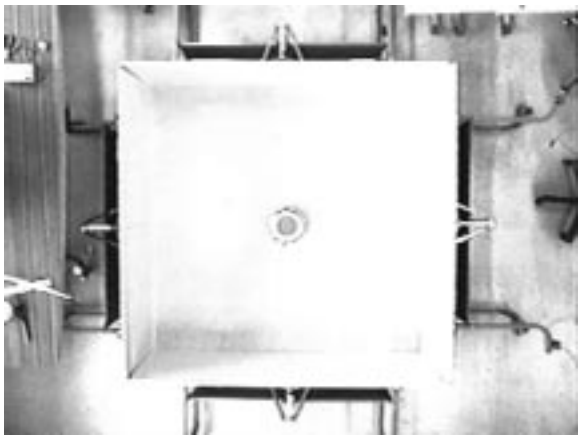

Fig. 15. Experimental environment.

state space of (8), became as follows:

$$\lambda_1 = 1.2 \times 10^{-2}$$
$$\lambda_2 = -6.6 \times 10^{-5}$$
$$\lambda_3 = -6.9 \times 10^{-4}.$$

The maximum exponent, λ_1, is positive and, therefore, the motion of robot possesses the sensitive dependence on initial conditions.

From the numerical computations, we can conclude that the motion of the robot due to the proposed controller is chaotic.

IV. Experiment

We made experiments using a two-wheeled mobile robot shown in Fig. 14 and setting up an experimental environment (1.8 m $\times$ 1.8 m) shown in Fig. 15. The robot has six proximity sensors at the front. The mirror mapping is applied based on the information.

The chaotic mobile robot ran with the following conditions:

$$linear\ velocity: v = 12\ [\text{cm/sec}]$$
$$coefficients: A = 0.27\ [1/\text{s}], B = 0.135\ [1/\text{s}],$$
$$C = 0.135\ [1/\text{s}]$$
$$initial\ states: x_1 = 4, x_2 = 3.5, x_3 = 0$$
$$period: \quad 2\ \text{hours}.$$

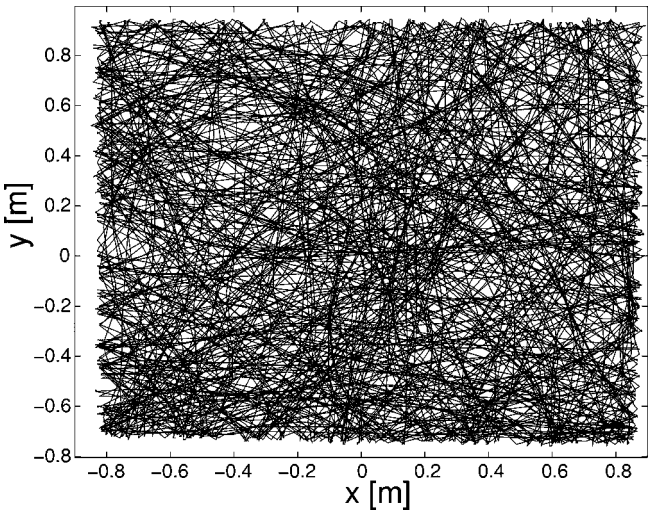

Fig. 16. Resultant trajectory of the experiment (chaotic robot).

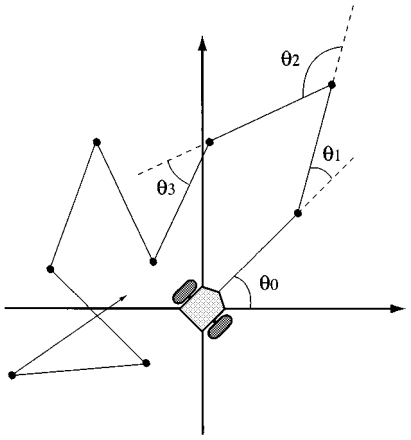

Fig. 17. Random walk.

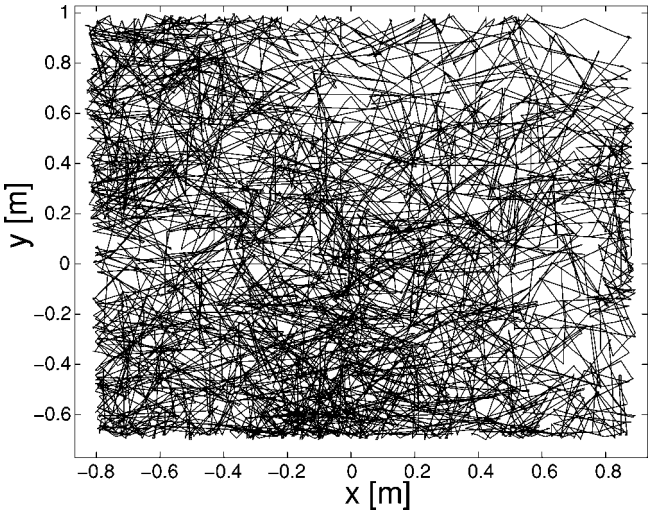

Fig. 18. Resultant trajectory of the experiment (random walk).

The result is shown in Fig. 16, which was obtained by tracking the robot using a camera above the experimental environment. The robot successfully scanned the whole workspace.

V. Discussion: Chaos Versus Randomness

Random walk is another method used to scan some workspace without the map. We need to discuss the usefulness of the chaotic

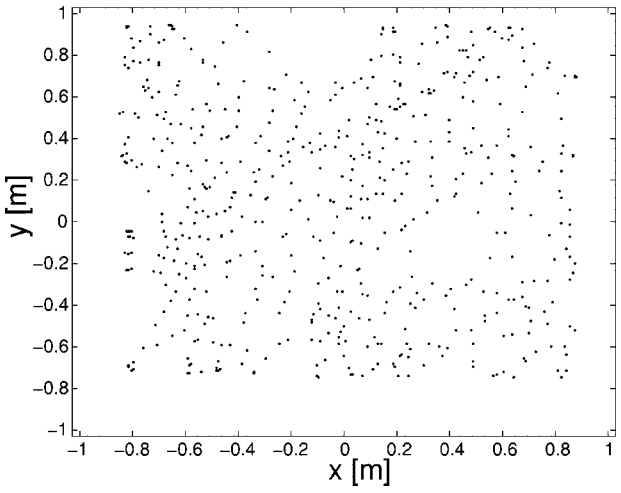

(a)

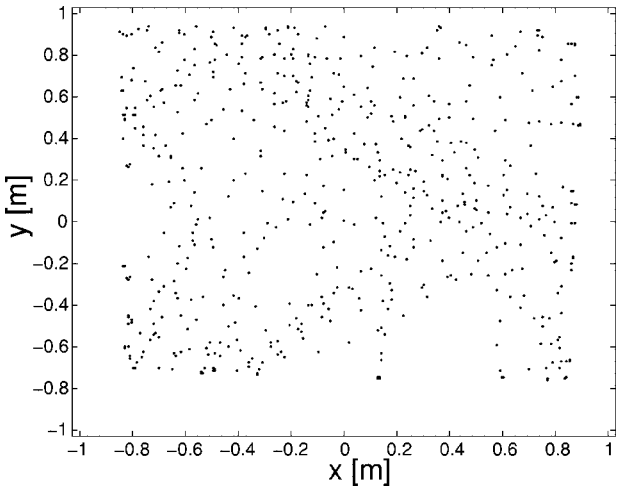

(b)

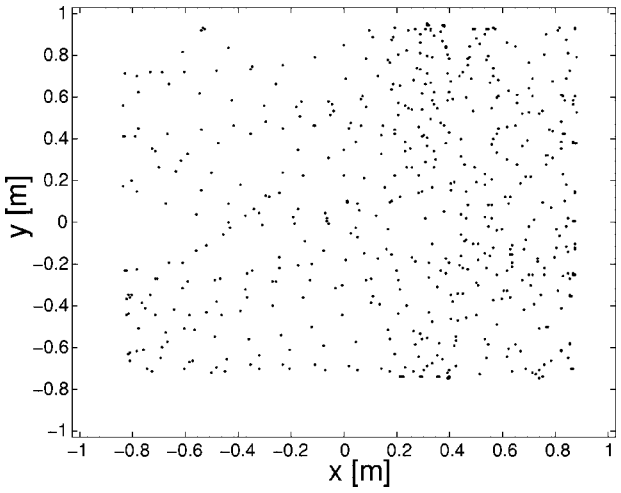

(c)

Fig. 19. Plots of robot position at 10-min intervals (chaotic robot). (a) t = 0–10 [min]. (b) t = 10–20 [min]. (c) t = 20–30 [min].

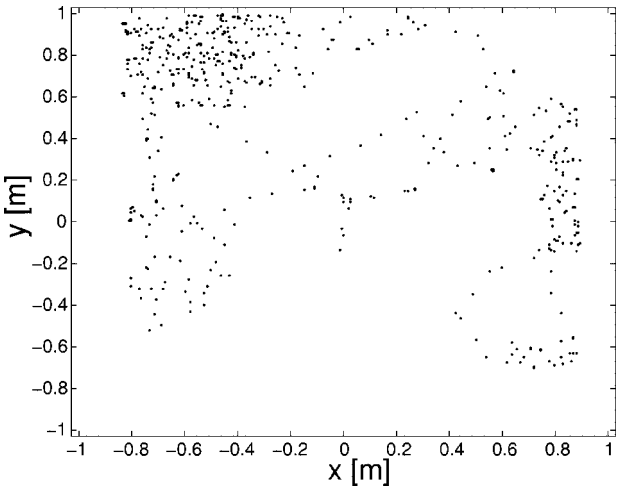

(a)

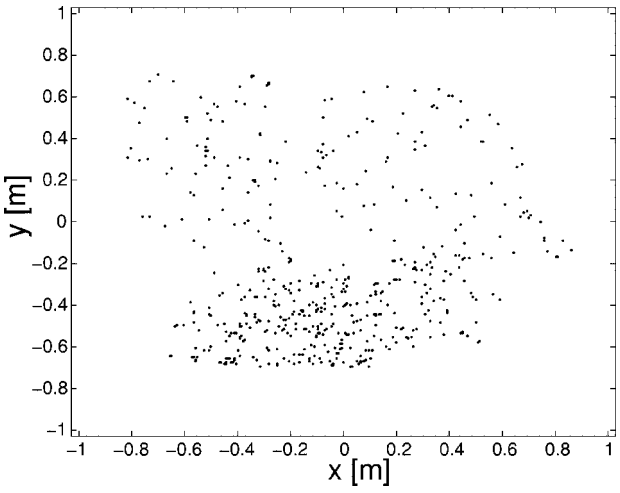

(b)

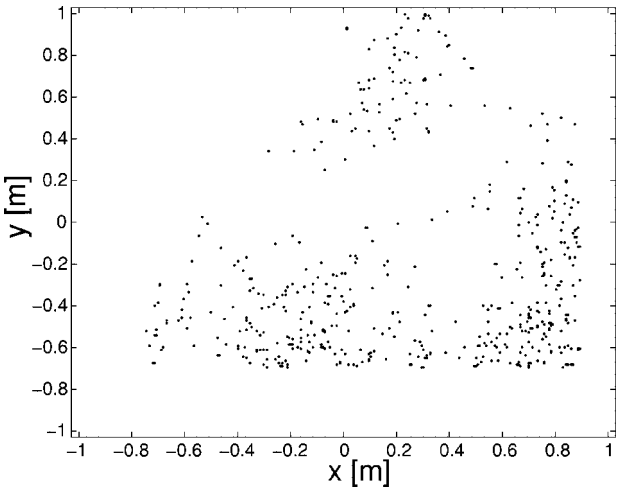

(c)

Fig. 20. Plots of robot position at 10-min intervals (random walk). (a) t = 0–10 [min]. (b) t = 10–20 [min]. (c) t = 20–30 [min].

mobile robot as compared with random walk. We also ran the robot for 2 h by using random walk. Random walk was implemented in such a way that the robot turns toward random direction after moving straight for every 2 s (Fig. 17). The experimental environment and the constant velocity of the robot were the same as those of the previous experiment. The mirror mapping was also applied at boundaries.

Fig. 18 shows the result. The density of resultant trajectory of random walk is lower than that of the chaotic robot because the robot must spend time to stop and turn after moving for 2 s. It is one of the advantages of the proposed controller that the robot can move continuously with the constant linear velocity.

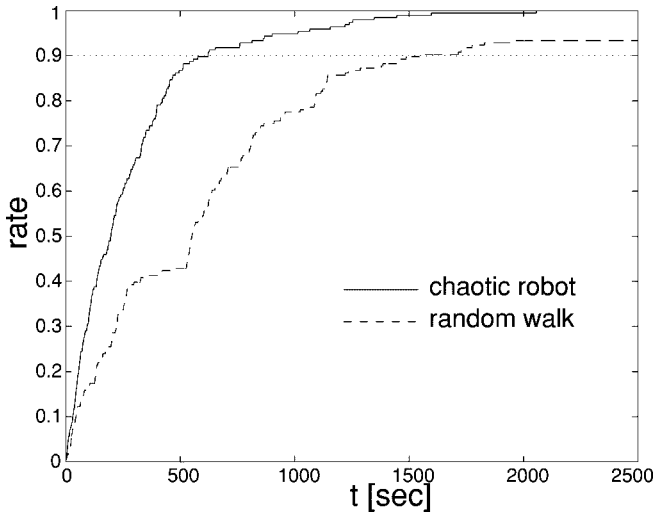

Fig. 21. Rate of covered area.

Figs. 19 and 20 are plots of the position of the robot after every 1 s during every 10 min. It can be seen that the chaotic mobile robot in Fig. 19 could scan the workspace more efficiently. The presented approach is not a method to plan a path to scan the whole workspace when its geometry is known, but rather a method to scan a workspace of which the geometry is unknown. Therefore, some areas might be covered many times before the robot covers the whole area. However, in our experiments, it can be seen that the density of coverage of the robot over its environment is uniform in the whole space since the points in Fig. 19 are scattered around the whole environment, while in the case of the random walk the density is not uniform in Fig. 20.

Fig. 21 shows the growth of the ratio of the covered area by the robot to the whole area. The chaotic mobile robot could cover 90% of the whole area in one third of the time taken by the random walk method to cover the same area.

There are many different ways to integrate random walk. Therefore, the above conclusion is not in any sense general. However, there is a possibility that the chaotic scan is stochastically superior to the scan by randomness. On the manifold integral calculus by the Monte Carlo method, Umeno [13] made a comparison between the algorithm using an exactly solvable chaos and the conventional algorithm using random numbers and showed superiority of the chaos computing. He explained that long-term correlation and the non-Gaussian nature of chaos could play important roles in this problem. Our problem of scanning the whole connected workspace is considered as a Monte Carlo computing to get the square measure of the workspace. The chaotic mobile robot has a chance being sperior to random walk, although the Arnold equation in the proposed controller is not an exactly solvable chaos. Our experiments with analysis of Figs. 19 and 20 clearly showed that the chaotic mobile robot is superior to an algorithm of random walk in efficiency of scanning the workspace.

VI. Conclusion

In this paper, we proposed the chaotic mobile robot, which implies a mobile robot with a controller that guarantees its chaotic motion.

The Arnold equation, which is known to show the chaotic behavior of noncompressive perfect fluid, was adopted as the chaotic dynamics to be integrated into the mobile robot and the behavior of the Arnold equation was analyzed. We designed the controller such that the total dynamics of the mobile robot is characterized by the Arnold equation. We proposed the mirror mapping, which is a method for an actual chaotic mobile robot of moving in spaces with boundaries like walls or obstacles. By the numerical analysis, it was illustrated that the behavior of the robot due to the proposed controller is chaotic. The experimental results illustrated the usefulness of the proposed controller.

References

[1] E. Ott, C. Grebogi, and J. A. Yorke, "Controlling chaos," *Phys. Rev. Lett.*, vol. 64, no. 11, pp. 1196–1199, 1990.
[2] T. Shinbrot, C. Grebogi, E. Ott, and J. A. Yorke, "Using small perturbations to control chaos," *Nature*, vol. 363, pp. 411–417, 1993.
[3] K. Cuomo, A. V. Oppenheim, and S. H. Strogatz, "Synchronization of lorenz-based chaotic circuits with application to communications," *IEEE Trans. Circuits Syst. II*, vol. 40, pp. 626–633, Oct. 1993.
[4] T. Ushio, "Chaotic synchronization and controlling chaos based on contraction mappings," *Phys. Lett. A*, vol. 198, no. 1, pp. 14–22, 1995.
[5] K. Aihara, T. Takabe, and M. Toyoda, "Chaotic neural networks," *Phys. Lett. A*, vol. 144, no. 6,7, pp. 333–340, 1990.
[6] Y. Yao and W. J. Freeman, "Model of biological pattern recognition with spatially chaotic dynamics," *Neural Networks*, vol. 3, pp. 153–170, 1990.
[7] I. Tsuda, "Can stochastic renewal of maps be a model for cerebral cortex?," *Physica D*, vol. 75, pp. 165–178, 1994.
[8] I. Tokuda, T. Nagashima, and K. Aihara, "Global bifurcation structure of chaotic neural networks and its application to traveling salesman problems," *Neural Networks*, vol. 10, no. 9, pp. 1673–1690, 1997.
[9] H. Okamoto and H. Fujii, *Nonlinear Dynamics, Iwanami Lectures of Applied Mathematics* (in Japanese) Iwanami, Tokyo, 1995, vol. 14.
[10] S. Wiggins, *Introduction to Applied Nonlinear Dynamical Systems and Chaos*: Springer-Verlag, 1990.
[11] G. L. Baker and J. P. Gollub, *Chaotic Dynamics an Introduction*. Cambridge, U.K.: Cambridge Univ. Press, 1990.
[12] I. Shimada and T. Nagashima, "A numerical approach to ergodic problem of dissipative dynamical systems," *Prog. Theor. Phys.*, vol. 61, no. 6, pp. 1605–1616, 1979.
[13] K. Umeno, "Chaos and computing" (in Japanese), *Math. Sci.*, no. 415, pp. 60–68, Jan. 1998.